

# Centrality dependence of light (anti)nuclei and (anti)hypertriton production in Au+Au collisions at $\sqrt{s_{NN}} = 200$ GeV

Gang Chen\*, Huan Chen, Juan Wu, De-Sheng Li and Mei-Juan Wang  
*School of Mathematics and Physics, China University of Geoscience, Wuhan 430074, China.*

We have used the dynamically constrained phase space coalescence model to investigate the centrality dependence of light (anti)nuclei and (anti)hypertriton production based on the  $6.2 \times 10^7$  hadronic final states generated by the PACIAE model in Au+Au collisions at  $\sqrt{s_{NN}} = 200$  GeV in  $|y| < 1$  and  $p_T < 5$  acceptances. It turned out that the yields of light (anti)nuclei and (anti)hypertriton strongly depend on the centrality, i.e. their yields decrease rapidly with the increase of centrality bins; but their yield ratios are independent on centrality. These theoretical results are consistent with the STAR and PHENIX data. Furthermore, centrality distribution of  $d$  ( $\bar{d}$ ),  ${}^3\text{He}$  ( ${}^3\bar{\text{He}}$ ) and  ${}^3_\Lambda\text{H}$  ( ${}^3_\Lambda\bar{\text{H}}$ ) follows Gaussian distributions. This means that light (anti)nuclei and (anti)hypertriton are primarily produced in the central collisions.

PACS numbers: 25.75.-q, 24.85.+p, 24.10.Lx

## I. INTRODUCTION

Ordinary matter and antimatter asymmetry is a fundamental problem in modern physics research. Since C. D. Anderson discovered the first antiparticle, i.e. positron, inside the cosmic rays in 1932, then the anti-neutrons, anti-protons and other anti-particles and light (anti)nuclei have gradually been discovered in scientific experiments [1–6]. It is believed that there exists equal amount of ordinary matter and antimatter in the initial stages of the universe. Especially, after the discovery of the first hypernuclei in 1952 [7], searching for (anti)hypernuclei bound states and exploring the hyperon-nucleon interaction have been steadily fascinating the sights of nuclear physicists [8, 9]. Because an anti-nucleus is very unstable and its yield is very low, so the progress of antimatter research was slow. In the high energy collision experiments, the high temperature and high baryon density matter is similar to the "Fireball" environment produced in the initial stages of the Big Bang, which is uniquely suitable for the production of both the light (anti)nuclei and (anti)hypernuclei mentioned above.

The STAR collaboration has reported their measurements of  ${}^3_\Lambda\text{H}$ ,  ${}^3_\Lambda\bar{\text{H}}$  and  ${}^4\bar{\text{He}}$  in Au+Au collisions at the top RHIC energy [8, 9]. The ALICE collaboration has also published their preliminary  $\bar{d}$  yield of  $\sim 6 \times 10^{-5}$  measured in the pp collisions at  $\sqrt{s} = 7$  TeV [10, 11].

On the other hand, the theoretical study of light nuclei (anti-nuclei) is usually divided into two steps. Firstly the nucleons and hyperons are calculated with some selected models, such as the transport models. Then the light nuclei (anti-nuclei) are calculated by the phase space coalescence model [12–14] and/or the statistical model [15, 16] etc. Recently, the production of light nuclei (hypernuclei) in the Au+Au/Pb+Pb collisions

at relativistic energies has been investigated theoretically by the coalescence+blast-wave method [17] and the UrQMD-hydro hybrid model+thermal model [18], respectively.

Besides, we have proposed an approach, PACIAE + the dynamically constrained phase-space coalescence model (DCPC model) [19]. DCPC is based on the final hadronic state generated by a parton and hadron cascade model PACIAE [20]. We have first predict the light nuclei (anti-nuclei) yield, transverse momentum distribution, and the rapidity distribution in non-single diffractive pp collisions at  $\sqrt{s} = 7$  TeV [19]. Then we use this method to investigate the light nuclei (anti-nuclei) and hypernuclei (anti-hypernuclei) productions for in 0-5% most central Au+Au collisions at  $\sqrt{s_{NN}} = 200$  GeV [21].

It should be noted that the results of light (anti)nuclei and (anti)hypernuclei yields and their ratios given by different experimental groups employed event samples with different centralities. For example, the STAR analysis in ref. [22] used a data sample of 25 million central triggered events (0-12% centrality) plus 24 million minimum-bias triggered events (0-80% centrality). For STAR in ref. [8], about 89 million collision events were collected using minimum-bias events, and an additional 22 million events were collected using near-zero impact parameter collisions. The data set for PHENIX analysis in ref. [5] includes  $21.6 \times 10^6$  minimum bias events. In theoretical studies, the production of light (anti)nuclei and (anti)hypernuclei is usually investigated in most central heavy ion collisions events (0-5% centrality) [17–19, 21]. However, in previous theoretical and experimental studies, little attention has been paid to the impact of the centrality on the production for light (anti)nuclei and (anti)hypernuclei in heavy ion collisions. In fact, the centrality in heavy ion collisions may have a great impact on the yields of light (anti)nuclei. In order to effectively compare the experimental and theoretical results for different collision centralities, it is necessary to study the dependence of light (anti)nuclei and (anti)hypernuclei yields as well as their ratios on the centrality in detail.

\*Corresponding Author: chengang1@cug.edu.cn

The paper is organized as follows: In Sec. II, we briefly introduce the PACIAE model and the dynamically constrained phase-space coalescence model (DCPC model). In Sec. III, the numerical results of light (anti)nuclei and (anti)hypernuclei yields and their ratios are given in different centrality bins, and are compared with the STAR and PHENIX data. A short summary is the content of Sec. IV.

## II. MODELS

The PYTHIA model (PYTHIA 6.4 [23]) is devised for the high energy hadron-hadron ( $hh$ ) collisions. In this model, a  $hh$  collision is decomposed into parton-parton collisions. The hard parton-parton scattering is described by the leading order perturbative QCD (LO-pQCD) parton-parton interactions with a modification of parton distribution function in a hadron. For the soft parton-parton collision, a non-perturbative process is considered empirically. The initial- and final-state QCD radiations and the multiparton interactions are also taken into account. Therefore, the consequence of a  $hh$  collision is a partonic multijet state composed of di-quarks (anti-diquarks), quarks (antiquarks) and gluons, as well as a few hadronic remnants. This is then followed by the string construction and fragmentation. A hadronic final state is obtained for a  $hh$  collision eventually.

The parton and hadron cascade model PACIAE [20] is based on PYTHIA 6.4 and is devised mainly for the nucleus-nucleus collisions. In the PACIAE model, firstly, the nucleus-nucleus collision is decomposed into the nucleon-nucleon (NN) collisions according to the collision geometry and NN total cross section. Each NN collision is described by the PYTHIA model with the string fragmentation switches-off and di-quarks (anti-diquarks) randomly breaks into quarks (anti-quarks). So the consequence of a NN collision is a partonic initial state composed of quarks, anti-quarks, and gluons. Provided all NN collisions are exhausted, one obtains a partonic initial state for a nucleus-nucleus collision. This partonic initial state is regarded as the quark-gluon matter (QGM) formed in the relativistic nucleus-nucleus collisions. Secondly, the parton rescattering proceeds. The rescattering among partons in QGM is randomly considered by the  $2 \rightarrow 2$  LO-pQCD parton-parton cross sections [24]. In addition, a  $K$  factor is introduced here to account for higher order and non-perturbative corrections. Thirdly, the hadronization happens after the parton rescattering. The partonic matter can be hadronized by the Lund string fragmentation regime [23] and/or the phenomenological coalescence model [20]. Finally, the hadronic matter proceeds rescattering until the hadronic freeze-out (the exhaustion of the hadron-hadron collision pairs). We refer to [20] for the details.

In quantum statistical mechanics [25] one can not precisely define both position  $\vec{q} \equiv (x, y, z)$  and momentum

$\vec{p} \equiv (p_x, p_y, p_z)$  of a particle in the six dimension phase space, because of the uncertainty principle

$$\Delta\vec{q}\Delta\vec{p} \leq h^3.$$

We can only say that this particle lies somewhere within a six dimension quantum "box" or "state" with a volume of  $\Delta\vec{q}\Delta\vec{p}$ . A particle state occupies a volume of  $h^3$  in the six dimension phase space [25]. Therefore one can estimate the yield of a single particle by defining the following integral

$$Y_1 = \int_{H \leq E} \frac{d\vec{q}d\vec{p}}{h^3}, \quad (1)$$

where  $H$  and  $E$  are the Hamiltonian and energy of the particle, respectively. Similarly, the yield of  $N$  particle cluster can be estimated as following integral

$$Y_N = \int \dots \int_{H \leq E} \frac{d\vec{q}_1 d\vec{p}_1 \dots d\vec{q}_N d\vec{p}_N}{h^{3N}}. \quad (2)$$

Therefore the yield of  $\frac{3}{\Lambda}H$  in the dynamically constrained phase space coalescence model, for instance, is assumed to be

$$Y_{\frac{3}{\Lambda}H} = \int \dots \int \delta_{123} \frac{d\vec{q}_1 d\vec{p}_1 d\vec{q}_2 d\vec{p}_2 d\vec{q}_3 d\vec{p}_3}{h^9}, \quad (3)$$

where

$$\delta_{123} = \begin{cases} 1 & \text{if } 1 \equiv \bar{p}, 2 \equiv \bar{n}, 3 \equiv \bar{\Lambda}, \\ & m_0 \leq m_{inv} \leq m_0 + \Delta m, \\ & q_{12} \leq D_0, \quad q_{13} \leq D_0, \quad q_{23} \leq D_0, \\ 0 & \text{otherwise,} \end{cases} \quad (4)$$

$$m_{inv} = [(E_1 + E_2 + E_3)^2 - (\vec{p}_1 + \vec{p}_2 + \vec{p}_3)^2]^{1/2}, \quad (5)$$

and  $(E_1, E_2, E_3)$  and  $(\vec{p}_1, \vec{p}_2, \vec{p}_3)$  are the energies and momenta of particles  $\bar{p}, \bar{n}, \bar{\Lambda}$ , respectively. In Eq. (4),  $m_0$  and  $D_0$  stand for, respectively, the rest mass and diameter of  $\frac{3}{\Lambda}H$ ,  $\Delta m$  refers to the allowed mass uncertainty, and  $q_{ij} = |\vec{q}_i - \vec{q}_j|$  is the vector distance between particle  $i$  and  $j$ .

As the hadron position and momentum distributions from transport model simulations are discrete, the integral over continuous distributions in Eq. (3) should be replaced by the sum over discrete distributions. In a single event of the final hadronic state obtained from transport model simulation, the configuration of  $\frac{3}{\Lambda}H$  ( $\bar{p} + \bar{n} + \bar{\Lambda}$ ) system, for instance, can be expressed as

$$C_{\bar{p}\bar{n}\bar{\Lambda}}(\Delta q_1, \Delta q_2, \Delta q_3; \vec{p}_1, \vec{p}_2, \vec{p}_3), \quad (6)$$

where the subscripts  $1 \equiv \bar{p}$ ,  $2 \equiv \bar{n}$ ,  $3 \equiv \bar{\Lambda}$ , and  $\Delta q_i$  refers to the distance between particle  $i$  and center-of-mass of three particles, ie.

$$\Delta q_i = |\vec{q}_i - \vec{q}_c|, \quad (i = 1, 2, 3). \quad (7)$$

Here,  $\vec{q}_c$  is the coordinate vector of the center-of-mass of  $\bar{p}$ ,  $\bar{n}$ , and  $\bar{\Lambda}$ . Therefore the third constraint (diameter constraint) in Eq. (4) is correspondingly replaced by

$$\Delta q_1 \leq R_0, \quad \Delta q_2 \leq R_0, \quad \Delta q_3 \leq R_0, \quad (8)$$

where  $R_0$  refers to the radius of  $\frac{3}{\Lambda}\bar{H}$ .

Each of the above configurations contributes a partial yield of

$$y_{\bar{p}\bar{n}\bar{\Lambda}} = \begin{cases} 1 & \text{if } m_0 \leq m_{inv} \leq m_0 + \Delta m, \\ & \Delta q_1 \leq R_0, \quad \Delta q_2 \leq R_0, \quad \Delta q_3 \leq R_0; \\ 0 & \text{otherwise;} \end{cases} \quad (9)$$

to the yield of  $\frac{3}{\Lambda}\bar{H}$ . So the total yield of  $\frac{3}{\Lambda}\bar{H}$  in a single event is the sum of the above partial yield over the configuration in Eq. (6) and their combinations. An average yield for all the events is required at the end.

### III. THE RESULTS AND DISCUSSES

Firstly we produce the final state particles using the PACIAE model. In the PACIAE simulations we assume that hyperons heavier than  $\Lambda$  decay already. The model parameters are fixed on the default values given in PYTHIA [23]. However, the K factor as well as the parameters  $\text{parj}(1)$ ,  $\text{parj}(2)$ , and  $\text{parj}(3)$ , relevant to the strange production in PYTHIA [23], are given by fitting the STAR data of  $\Lambda$ ,  $\bar{\Lambda}$ ,  $\Xi^-$ , and  $\bar{\Xi}^-$  in Au+Au collisions at  $\sqrt{s_{NN}} = 200$  GeV [26]. The fitted parameters of  $K=3$  (default value is 1 or 1.5 [23]),  $\text{parj}(1)=0.12$  (0.1),  $\text{parj}(2)=0.55$  (0.3), and  $\text{parj}(3)=0.65$  (0.4) are used to generate  $6.2 \times 10^7$  events (final hadronic states) by the PACIAE model. A minimum-bias events sample is formed in Au+Au collisions at  $\sqrt{s_{NN}} = 200$  GeV of  $|y| < 1$  and  $0 < p_t < 5$  acceptances.

Fig. 1 shows the strange particle yields (open symbols) calculated with the PACIAE model at the midrapidity for different centralities Au+Au collisions at  $\sqrt{s_{NN}} = 200$  GeV. The solid symbols in this figure are the experimental data taken from [26]. One sees in this figure that the PACIAE results agree well with the experimental data.

Then, the yields of  $d$  ( $\bar{d}$ ),  ${}^3\text{He}$  ( ${}^3\bar{H}e$ ), as well as  $\frac{3}{\Lambda}\bar{H}$  ( $\frac{3}{\Lambda}\bar{H}$ ) and their ratios are calculated by the DCPC model for different centrality bins of 0-5%, 0-12%, 0-30%, 0-50%, 0-80% and 0-100%. The subsamples of collision events in different centrality bins are identified by the impact parameter  $b$  in PACIAE model from the minimum-bias event sample.

In Fig. 2 we show the yield distributions of  $d$ ,  $\bar{d}$ ,  $\frac{3}{\Lambda}\bar{H}$ ,  ${}^3\text{He}$ , and  ${}^3\bar{H}e$  in different centralities Au+Au collisions at  $\sqrt{s_{NN}} = 200$  GeV. The upper panel is for  $d$  ( $\bar{d}$ ), the lower panel is for  $\frac{3}{\Lambda}\bar{H}$  ( $\frac{3}{\Lambda}\bar{H}$ ) and  ${}^3\text{He}$  ( ${}^3\bar{H}e$ ). For comparison, the figure also exhibits the experimental data with solid symbols. It can be seen from Fig. 2

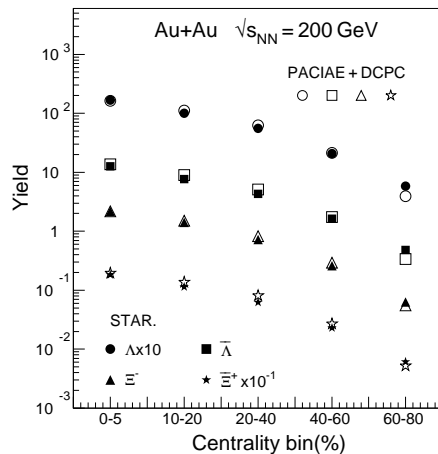


FIG. 1: Yields of strange particle at midrapidity ( $|y| < 1$  for  $\Lambda$  and  $\bar{\Lambda}$ ,  $|y| < 0.75$  for  $\Xi^-$  and  $\bar{\Xi}^-$ ) in the Au+Au collisions at  $\sqrt{s_{NN}} = 200$  GeV as a function of centrality bin. The open symbols represent our model results and the solid symbols are the data points from STAR [26].

that the yields of light (anti)nuclei and (anti)hypertriton all decrease rapidly with the centrality bins; the PACIAE+DCPC model results (the open symbols) are in agreement with the STAR [8, 22] and PHENIX [5] data (the solid symbols).

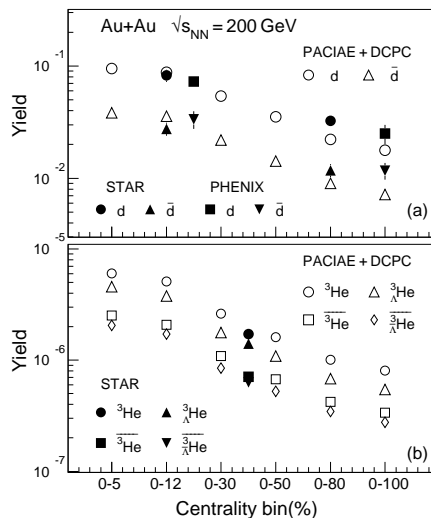


FIG. 2: The comparison of yields for light (anti)nuclei and (anti)hypertriton between model results and experimental data at midrapidity in the Au+Au collisions at  $\sqrt{s_{NN}} = 200$  GeV, plotted as a function of centrality bin. The open symbols represent our model results. The solid symbols are the data points from STAR [8, 22] and PHENIX [5]. Panel (a) is for  $\bar{d}$  and  $d$ , and panel (b) is for  $\frac{3}{\Lambda}\bar{H}$ ,  $\frac{3}{\Lambda}H$ ,  ${}^3\bar{H}e$  and  ${}^3He$ .

In Tab. I the yield ratios of light antinuclei and antihypertriton to light nuclei and hypertriton, as well as  $\frac{3}{\Lambda}\bar{H}$  to  ${}^3He$  and  $\frac{3}{\Lambda}\bar{H}$  to  ${}^3\bar{H}e$  are given in different centralities

TABLE I: The yield ratios in different centrality bins from Au+Au collisions at  $\sqrt{s_{\text{NN}}} = 200$  GeV, comparing with PHENIX and STAR data.

Ratio	$R_{\text{PACIAE+DCPC}}^a$						$R_{\text{STAR}}$			$R_{\text{PHENIX}}$		
	Centrality(%)	0-5	0-12	0-30	0-50	0-80	0-100	0-12	0-80	mixed	0-20	0-100
$\bar{d}/d$	0.402	0.406	0.406	0.405	0.405	0.405	0.394 <sup>b</sup>	0.428 <sup>b</sup>	—	—	0.462 <sup>d</sup>	0.468 <sup>d</sup>
${}^3\text{He}/{}^3\text{He}$	0.418	0.407	0.416	0.417	0.419	0.419	—	—	0.45±0.18 ± 0.07 <sup>c</sup>	—	—	—
$\frac{3}{\Lambda}\bar{H}/\frac{3}{\Lambda}H$	0.451	0.455	0.480	0.481	0.507	0.507	—	—	0.49±0.18 ± 0.07 <sup>c</sup>	—	—	—
$\frac{3}{\Lambda}H/{}^3\text{He}$	0.756	0.739	0.674	0.677	0.677	0.677	—	—	0.82±0.16 ± 0.32 <sup>c</sup>	—	—	—
$\frac{3}{\Lambda}\bar{H}/{}^3\bar{H}$	0.817	0.826	0.778	0.782	0.819	0.819	—	—	0.89±0.28 ± 0.13 <sup>c</sup>	—	—	—

<sup>a</sup> calculated with  $\Delta m=0.0003$  GeV for  $d, \bar{d}$  and  $\Delta m=0.0002$  GeV for  ${}^3\text{He}, {}^3\text{He}, \frac{3}{\Lambda}\bar{H}$  and  $\frac{3}{\Lambda}H$ .

<sup>b</sup> taken from Fig. 2 in [22].

<sup>c</sup> taken from [8] calculated with 89 million minimum-bias events and 22 million central collision events.

<sup>d</sup> taken from [5].

Au+Au collisions at  $\sqrt{s_{\text{NN}}} = 200$  GeV. For comparison, experimental results from STAR and PHENIX are also given in Tab. I. One can see in this table that the yield ratios in different centrality bins remain unchanged although their yields decrease rapidly with the centrality bin as shown Fig. 2, and the results obtained from our model are in agreement with the experimental data from STAR [8, 22] and PHENIX [5].

In order to further analyze the centrality dependence of light (anti)nuclei generation, the centrality distributions of particle yield for  $d, \bar{d}, \frac{3}{\Lambda}H, \frac{3}{\Lambda}\bar{H}, {}^3\text{He}$  and  ${}^3\bar{H}$  in Au+Au collisions at  $\sqrt{s_{\text{NN}}} = 200$  GeV, calculated by the PACIAE+DCPC model, are given in Fig. 3. It shows that the centrality distributions of particle yield are similar for six kinds of particles. Their yields have a maximum peak nearby centrality  $C = 0$ , and fall rapidly with the increase of centrality until they approach zero at centralities  $C$  greater than about 40%. This indicates that the yield of the light (anti)nuclei and (anti)hypertriton is strongly dependent on the centrality, i.e. the light (anti)nuclei and (anti)hypertriton are generated primarily in central collision region, and their yields in peripheral collision are almost negligible.

Quantitatively, the results are in accord with the Gaussian distributions, i.e.

$$\frac{1}{N} \frac{dN}{dC} = \alpha \exp\left(-\frac{C^2}{2\sigma^2}\right). \quad (10)$$

The fitted parameters  $\alpha$  and  $\sigma$  corresponding to different particles are shown in Tab. II. We can further obtain that the value of  $3\sigma$  is  $(44.7 \pm 1.2)\%$  for  $d$ ,  $(47.7 \pm 1.2)\%$  for  $\bar{d}$ ,  $(35.1 \pm 1.2)\%$  for  ${}^3\text{He}$ ,  $(37.2 \pm 0.9)\%$  for  ${}^3\bar{H}$ ,  $(34.2 \pm 1.2)\%$  for  $\frac{3}{\Lambda}H$  and  $(36.6 \pm 0.9)\%$  for  $\frac{3}{\Lambda}\bar{H}$ .

In order to effectively compare the theoretical and experimental results for different centrality bins, we define a normalized yield  $y_i$  as

$$y_i \equiv \frac{Y_i}{Y_{\text{MB}}}, \quad (11)$$

where  $Y_i$  is the yield in the  $i$ -th centrality bin,  $Y_{\text{MB}}$  is the yield in minimum-bias events. The normalized yield

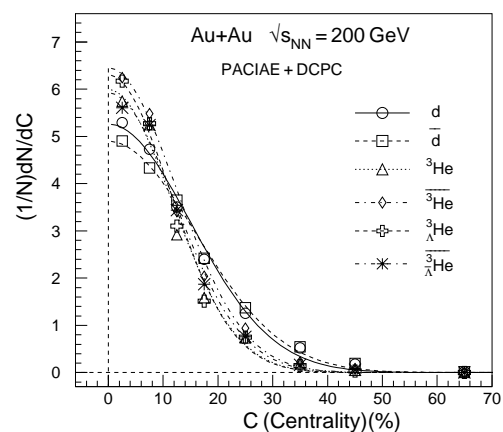


FIG. 3: Centrality distribution of particle yields  $dN/dC/N$  for light (anti)nuclei and (anti)hypertriton ( $d, \bar{d}, \frac{3}{\Lambda}H, \frac{3}{\Lambda}\bar{H}, {}^3\text{He}$  and  ${}^3\bar{H}$ ) at midrapidity in Au+Au collisions at  $\sqrt{s_{\text{NN}}} = 200$  GeV. The results are obtained by the PACIAE+DCPC model. The curves are fitted by the Gaussian distribution Eq.(10)

$y_i$  for  $\bar{d}, d, \frac{3}{\Lambda}\bar{H}, \frac{3}{\Lambda}H, {}^3\bar{H}$  and  ${}^3\text{He}$  in Au+Au collisions at  $\sqrt{s_{\text{NN}}} = 200$  GeV are given in Fig. 4. In this figure the curve is a function of

$$y_i = \frac{Y_i}{Y_{\text{MB}}} = \gamma \frac{1 - \Delta C}{\beta + \Delta C^2} + 1, \quad (12)$$

fit to the data points. In the equation,  $\gamma$  and  $\beta$  are parameters. It can be seen in Fig. 4 that the normalized yields  $y_i$  for light (anti)nuclei and (anti)hypertriton also decrease rapidly with the increase of centrality bins until they approach 1 at  $\Delta C = 1$ , i.e.  $y_i = Y_{\text{MB}} \equiv 1$ .

Setting the  $y_i$  distribution as a reference calibration curve, the yields in any centrality bins can be translated into the constant yield  $Y_{\text{MB}}$  corresponding to its minimum-bias events according to Eq.(11). Thus theoretical and experimental results in different centralities heavy ion collisions can be directly compared.

TABLE II: The parameters  $\alpha$  and  $\sigma$  fitted by Eq.(10) with Fig. 3.

par.	d	$\bar{d}$	${}^3\text{He}$	${}^3\overline{\text{He}}$	${}^3_{\Lambda}\text{H}$	${}^3_{\Lambda}\overline{\text{H}}$
$\alpha$	$5.26 \pm 0.15$	$4.85 \pm 0.15$	$6.00 \pm 0.17$	$6.36 \pm 0.16$	$6.32 \pm 0.17$	$5.92 \pm 0.16$
$\sigma$	$0.149 \pm 0.004$	$0.159 \pm 0.004$	$0.117 \pm 0.004$	$0.124 \pm 0.003$	$0.114 \pm 0.004$	$0.122 \pm 0.003$

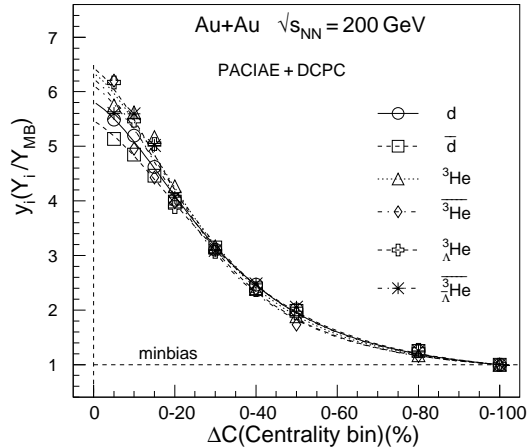


FIG. 4: The normalized yield  $y_i$  for the  $\bar{d}$ ,  $d$ ,  ${}^3_{\Lambda}\overline{\text{H}}$ ,  ${}^3_{\Lambda}\text{H}$ ,  ${}^3\overline{\text{He}}$  and  ${}^3\text{He}$  as a function of centrality bin. The results are calculated by PACIAE+DCPC model at midrapidity in the Au+Au collisions at  $\sqrt{s_{\text{NN}}} = 200$  GeV. The curves are fitted by Eq.(12).

#### IV. CONCLUSION

In this paper we use PACIAE+DCPC model to investigate the centrality dependence of light (anti)nuclei and

(anti)hypertriton production in Au+Au collisions at top RHIC energy. The results show that the yields of  $d$ ,  $\bar{d}$ ,  ${}^3_{\Lambda}\overline{\text{H}}$ ,  ${}^3_{\Lambda}\text{H}$ ,  ${}^3\overline{\text{He}}$ , and  ${}^3\text{He}$  decrease rapidly with the increase of centrality bins. However, the yield ratios of  $\bar{D}$  to  $D$ ,  ${}^3_{\Lambda}\overline{\text{H}}$  to  ${}^3_{\Lambda}\text{H}$  and  ${}^3\overline{\text{He}}$  to  ${}^3\text{He}$ , as well as  ${}^3_{\Lambda}\overline{\text{H}}$  to  ${}^3\overline{\text{He}}$  and  ${}^3_{\Lambda}\text{H}$  to  ${}^3\text{He}$  are independent on centrality. The results obtained from our model are also consistent with the STAR and PHENIX data. Our models results also show that the light (anti)nuclei and (anti)hypertriton are primarily produced in central collision regions, and the dependence of the yields on centrality follows a Gaussian distributions with centrality  $C < 45\%$  for  $d$  ( $\bar{d}$ ),  $C < 35\%$  for  ${}^3\text{He}$  ( ${}^3\overline{\text{He}}$ ) and  ${}^3_{\Lambda}\text{H}$  ( ${}^3_{\Lambda}\overline{\text{H}}$ ). The yields in the peripherad collision events are almost negligible. By defining a normalized yield  $y_i$ , the theoretical and experimental results of yields in different centrality bins of heavy ion collisions can be converted into the constant yield  $Y_{MB}$  to be directly compared.

#### ACKNOWLEDGMENT

Finally, we acknowledge the financial support from Central Universities (GUGL 100237,120829,130249) in China. The authors thank Prof. Ben-Hao Sa and PH.D. YU-liang Yan for helpful discussions.

- 
- [1] B. Cork, G. R.Lambertson, O. Piccioni, W. A. Wenzel, Phys. Rev. **104**, 1193 (1956).
  - [2] D.E. Dorfan, J. Eades, L. M. Lederman, W. Lee, C. C. Ting, Phys. Rev. Lett.**14**, 1003 (1965).
  - [3] Y. M. Antipov et al., Yad. Fiz. **12** , 311 (1970).
  - [4] N. K. Vishnevsky et al., Yad.Fiz. **20**, 694 (1974).
  - [5] PHENIX Collaboration, S. S. Adler et al., Phys. Rev. Lett.,**94**, 122302 (2005).
  - [6] STAR Collaboration, B.I. Abelev et al., Phys. Lett. B **655**, 104 (2007).
  - [7] M. Danysz and J. Pniewski, Philos. Mag. **44** , 348 (1953).
  - [8] The STAR Collaboration, Science **328**, 58 (2010); arXiv:1003.2030v1.
  - [9] The STAR Collaboration, H. Agakishiev et al., Nature **473**, 353 (2011);
  - [10] N. Sharma, ALICE Collaboration,Acta Physica Polonica B **5(2)** 605(2012); arXiv:1104.3311v1.
  - [11] N. Sharma, ALICE Collaboration,J. Phys. G: Nucl. Part. Phys. **38** 124189 (2011); arXiv:1109.4836v1.
  - [12] R. Mattiello, H. Sorge, H. Stöcker, and W. Greiner, Phys. Rev. C **55** 1443 (1997).
  - [13] Lie-Wen Chen and Che Ming Ko, Phys. Rev. C **73** 044903 (2006).
  - [14] S. Zhang, J. H. Chen, H. Crawford, D. Keane, Y. G. Ma, and Z. B. Xu, Phys. Lett. B **684**, 224 (2010), and references therein.
  - [15] V. Topor Pop and S. Das Gupta, Phys. Rev. C **81** 054911 (2010), and references therein.
  - [16] A. Andronic, P. Braun-Munzinger, J. Stachel, and H. Stöcker, Phys.Lett. B **697** 203 (2011); arXiv:1010.2995v1.
  - [17] L. Xue, Y. G. Ma, J. H. Chen, and S. Zhang, Phys. Rev. C **85** 064912 (2012).
  - [18] J. Steinheimer, K. Gudima, A. Botvina, I. Mishustin, M. Bleicher, and H. Stoecker, Phys. Lett. B **714** 85(2012).
  - [19] Yu-Liang Yan, Gang Chen, Xiao-Mei Li, et al. Phys. Rev. C **85** 024907(2012).
  - [20] Ben-Hao Sa, Dai-Mei Zhou, Yu-Liang Ya, et al. Comput. Phys. Commun. **183**, 333 (2012); arXiv:1104.1238v1.
  - [21] Gang Chen, Yu-Liang Yan, Li De-Sheng, et al. Phys. Rev. C **86** 054910(2012).
  - [22] B. I. Abelev et al. (The STAR Collaboration), arXiv:0909.0566 [nucl-ex].
  - [23] T. Sjöstrand, S. Mrenna, and P. Skands, J. High Energy

- Phys. **JHEP05**, 026 (2006).
- [24] B. L. Combridge, J. Kripfgang, and J. Ranft, Phys. Lett. B **70**, 234 (1977).
- [25] K. Stowe, A introduction to thermodynamics and statistical mechanics, Combridge, 2007; R. Kubo, Statistical Mechanics, North-Holland Publishing Company, Amsterdam, 1965.
- [26] J. Adams et al.(STAR Collaboration), Phys. Rev. Lett. **98**, 062301 (2007)